

A 10 deg² Lyman α survey at $z = 8.8$ with spectroscopic follow-up: strong constraints on the luminosity function and implications for other surveys^{*}

Jorryt J. A. Matthee,^{1†} David Sobral,¹ A. M. Swinbank,² Ian Smail,² P. N. Best,³ Jae-Woo Kim,⁴ Marijn Franx,¹ Bo Milvang-Jensen⁵ and Johan Fynbo⁵

¹Leiden Observatory, Leiden University, PO Box 9513, NL-2300 RA Leiden, the Netherlands

²Institute for Computational Cosmology, Durham University, South Road, Durham DH1 3LE, UK

³SUPA, Institute for Astronomy, Royal Observatory of Edinburgh, Blackford Hill, Edinburgh EH9 3HJ, UK

⁴Center for the Exploration of the Origin of the Universe, Department of Physics and Astronomy, Seoul National University, Seoul 151-742, Korea

⁵Dark Cosmology Centre, Niels Bohr Institute, University of Copenhagen, Juliane Maries Vej 30, DK-2100 Copenhagen, Denmark

Accepted 2014 February 26. Received 2014 February 26; in original form 2013 December 6

ABSTRACT

Candidate galaxies at redshifts of $z \sim 10$ are now being found in extremely deep surveys, probing very small areas. As a consequence, candidates are very faint, making spectroscopic confirmation practically impossible. In order to overcome such limitations, we have undertaken the CF-HiZELS survey, which is a large-area, medium-depth near-infrared narrow-band survey targeted at $z = 8.8$ Lyman α ($\text{Ly}\alpha$) emitters (LAEs) and covering 10 deg² in part of the SSA22 field with the Canada–France–Hawaii Telescope (CFHT). We surveyed a comoving volume of 4.7×10^6 Mpc³ to a $\text{Ly}\alpha$ luminosity limit of 6.3×10^{43} erg s⁻¹. We look for $\text{Ly}\alpha$ candidates by applying the following criteria: (i) clear emission-line source, (ii) no optical detections (*ugriz* from CFHTLS), (iii) no visible detection in the optical stack (*ugriz* > 27), (iv) visually checked reliable NB_J and J detections and (v) $J - K \leq 0$. We compute photometric redshifts and remove a significant amount of dusty lower redshift line-emitters at $z \sim 1.4$ or 2.2. A total of 13 $\text{Ly}\alpha$ candidates were found, of which two are marked as strong candidates, but the majority have very weak constraints on their spectral energy distributions. Using follow-up observations with SINFONI/VLT, we are able to exclude the most robust candidates as LAEs. We put a strong constraint on the $\text{Ly}\alpha$ luminosity function at $z \sim 9$ and make realistic predictions for ongoing and future surveys. Our results show that surveys for the highest redshift LAEs are susceptible of multiple contaminations and that spectroscopic follow-up is absolutely necessary.

Key words: galaxies: evolution – galaxies: high-redshift – cosmology: observations – dark ages, reionization, first stars.

1 INTRODUCTION

Finding the first stars and galaxies is one of the most important tasks to test our understanding of galaxy formation in the early Universe. The current theoretical models of when and how these first galaxies were formed can only be tested and improved by reliable detections of galaxies at the highest redshifts. The confirmation of galaxies at a redshift of $z \sim 9$ –10 would also allow the study of the epoch of reionization of the Universe. Measurements of the cosmic microwave background place this epoch at $z \sim 10.6$ (Komatsu et al. 2011), while Fan et al. (2006) located the end of the reionization

epoch at a redshift of at least $z \sim 6$ by studying spectra of quasars at high redshift, where they found a lower limit to the neutral fraction of $\sim 10^{-3}$ – 10^{-2} .

A widely used technique to detect very distant galaxies is the Lyman-break technique (LBG), pioneered by Steidel et al. (1996, see also Guhathakurta, Tyson & Majewski 1990), which looks at a distinctive break in the UV spectrum of star-forming galaxies. More generally, one can use deep data in several broad-bands to derive a redshift probability distribution by fitting spectral energy distributions (SED) based on galaxy templates (e.g. McLure et al. 2011).

Using the Lyman-break method, candidate galaxies have been found at very high redshifts ($z \sim 7$; e.g. Bouwens et al. 2011; Finkelstein et al. 2012; McLure et al. 2012; Oesch et al. 2012) and even $z \sim 10$ (Bouwens et al. 2013; Ellis et al. 2013; Oesch et al. 2013), but the great majority of these are too faint to confirm

^{*}Based on observations obtained with WIRCam on the CFHT, OPTICON programme 2011BA016, 2012A019 and 2012BA022.

[†]E-mail: matthee@strw.leidenuniv.nl

spectroscopically. Lehnert et al. (2010) claimed the spectroscopic detection of a $z = 8.6$ Ly α (Ly α) line of a LBG in the *Hubble Ultra Deep Field*. However, Bunker et al. (2013) were unable to reproduce the detection with two independent sets of observations, leading to the suggestion that it could be an artefact. Brammer et al. (2013) found a tentative emission line that could be Ly α at $z = 12.12$ using the *Hubble Space Telescope* WFC3 grism, but this is only a $<3\sigma$ detection and could be a lower redshift interloper. Recently, Finkelstein et al. (2013) report the detection of an Ly α emission line in a $z = 7.51$ LBG, although the line is very close to a sky-line, making identification significantly more difficult. Other attempts have been made, but so far no $z > 7.5$ galaxy has been spectroscopically confirmed. There is a spectroscopic redshift determination of a $z = 8.2$ gamma-ray burst (Tanvir et al. 2009), but not for its host.

Another successful technique to detect very high redshift ($z \sim 4-7$) galaxies is the narrow-band (NB) technique, which targets Ly α emitters (LAEs; e.g. Pritchett 1994; Thompson, Djorgovski & Beckwith 1994; Thompson, Djorgovski & Trauger 1995; Hu & McMahon 1996; Cowie & Hu 1998; Hu, Cowie & McMahon 1998; Thommes et al. 1998; Rhoads et al. 2000, 2003, 2004; Fynbo, Møller & Thomsen 2001; Hu et al. 2002, 2004; Malhotra & Rhoads 2002, 2004; Fynbo et al. 2003; Ouchi et al. 2003, 2008; Taniguchi et al. 2005; Iye et al. 2006; Kashikawa et al. 2006; Shimasaku et al. 2006; Finkelstein et al. 2009; Ota et al. 2010; Hibon et al. 2011). Using the NB technique, one can search for sources with emission lines at specific redshifts, by looking at the excess the NB has over the broad-band. This way sources for which the continuum is too faint to be detected, can still be identified due to the bright emission lines. However, most emission-line galaxies detected in NB surveys are lower redshift interlopers such as H α and [O II] (e.g. Sobral et al. 2012), which have to be identified using multiwavelength observations. Because the NB is only sensitive to sources emitting in a small range of wavelengths, they can be used to look at a slice of redshifts and therefore a well-known comoving volume. Moreover, spectroscopic follow-up of high-redshift candidates is a priori easier for candidates detected by the NB technique, as these candidates will have strong emission lines. Currently, the most distant spectroscopically confirmed NB-selected LAE is at a redshift of 6.96 (Iye et al. 2006), which is detected with NB imaging from the Subaru telescope.

To observe even higher redshift galaxies, observations in the near-infrared are required. Unfortunately, at these wavelengths, there is significant foreground emission due to OH molecules in the Earth's atmosphere. Some OH windows exist at wavelengths where the atmosphere is transparent to radiation. It is possible to observe using NB filters in these windows very effectively and several filters have been developed for this purpose (see Fig. 1). Recent studies led to the identification of candidate LAEs at a redshift of $z = 7.7$, but none of these has been spectroscopically confirmed yet (Hibon et al. 2010; Tilvi et al. 2010; Clément et al. 2012; Krug et al. 2012; Jiang et al. 2013).

Some attempts at somewhat higher redshifts ($z \sim 9$) were made to detect Ly α (Willis & Courbin 2005; Cuby et al. 2007; Willis et al. 2008; Sobral et al. 2009). The properties of such galaxies would provide strong tests of current models of galaxy formation and evolution and even the confirmation of just one luminous LAE at this redshift will be suitable for the study of these sources way before the next generation of telescopes, such as *JWST* or the E-ELT.

Ly α radiation is much more attenuated by a neutral intergalactic medium (IGM) than an ionized IGM, so large samples of LAEs at these redshifts could be used to derive properties of the IGM at these early times.

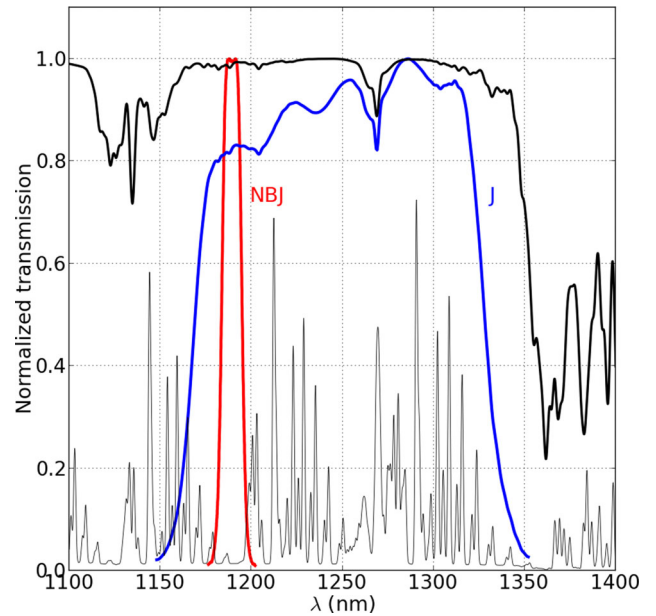


Figure 1. The atmospheric transmission in the near-infrared J band, normalized to the maximum transmission for each curve. Atmospheric data are from Mauna Kea, Gemini Observatory (Lord 1992), the airmass is 1.0 and water vapour column is 1.0 mm. The background (grey) atmospheric (OH) emission lines are also shown. The NB $_J$ filter used in this paper is transparent at wavelengths where there are no strong OH lines and also at wavelengths where the atmosphere is at its maximum transparency, thus allowing us to obtain deep observations in relatively little time.

Current simulations (e.g. Ilev et al. 2008) suggest that reionization started at the most overdense regions in the Universe, where ionizing sources nurtured expanding shells of ionized gas in the IGM. As Ly α radiation is easily absorbed by a neutral medium (Malhotra & Rhoads 2004), LAEs can only be observed once the ionized zone around them is large enough for the Ly α radiation to escape. This is expected to lead to a negative evolution in the Ly α luminosity function (LF) and dropping escape fraction of Ly α radiation at higher redshifts. Considerable effort has been put in spectroscopically studying the evolution of the Ly α line in Lyman-break galaxies (LBGs) at high redshifts (e.g. Fontana et al. 2010; Pentericci et al. 2011; Vanzella et al. 2011; Ono et al. 2012; Schenker et al. 2012; Caruana et al. 2013; Finkelstein et al. 2013). Recent non-confirmations and low success rates at $z > 7$ for their spectroscopic confirmation are interpreted as a signature that reionization is not yet completed at these redshifts. Treu et al. (2013), for example, find that at $z \sim 8$ Ly α emission of LBGs is suppressed by at least a factor of 3.

For LAEs, it is found that up to at least a redshift of $z \sim 6$, the Ly α LF is remarkably constant (e.g. Hu et al. 2004; Shimasaku et al. 2006; Ouchi et al. 2008). This indicates that LAEs are relatively more common and more luminous at earlier epochs, compared to LBGs (as the UV LF drops quickly in this redshift range; Bouwens et al. 2007). At $z \sim 6-8$, there is evidence for evolution of the characteristic luminosity, but these samples, including failed attempts at $z = 7.7$, can be significantly affected by cosmic variance, probing $\lesssim 1 \text{ deg}^2$ (e.g. Ouchi et al. 2010; Clément et al. 2012).

At the bright end, however, the evolution could plausibly be very different. Luminous sources can ionize their own surroundings to allow Ly α photons to escape, as they redshift out of rest-frame-resonance wavelength in about 1 Mpc (e.g. Cen & Haiman 2000; Barton et al. 2004; Curtis-Lake et al. 2012). Furthermore, the

observed clustering of LAEs is expected to increase at higher redshift, as neighbouring sources will have larger overlapping ionized spheres and therefore a higher fraction of escaped Ly α photons (e.g. Ouchi et al. 2010).

In order to find the most luminous LAEs in the epoch of reionization which would be suitable for spectroscopic follow-up, we have undertaken the widest area search with a near-infrared NB filter to date. This paper is organized in the following way. Section 2 presents the details of the observations, and describes the data reduction, calibrations and source extraction. Section 3 presents the criteria for sources being selected as Ly α candidates and the results from the NB search. Section 4 presents the spectroscopic follow-up observations and results. Section 5 discusses the results such as constraints on the Ly α $z = 8.8$ LF, and our survey is compared to past and future surveys. Finally, Section 6 outlines the conclusions. A $H_0 = 70 \text{ km s}^{-1} \text{ Mpc}^{-1}$, $\Omega_M = 0.3$ and $\Omega_\Lambda = 0.7$ cosmology is used and all magnitudes are in the AB system, except if noted otherwise.

2 NARROW-BAND OBSERVATIONS AND DATA REDUCTION

During 2011 September–December and 2012 October–November, we obtained medium-depth NB J photometry ($\text{NB}_J = 22.2$, 5σ , $F_{\text{lim}} = 1 \times 10^{-16} \text{ erg s}^{-1} \text{ cm}^{-2}$, pure emission line) over a 10 deg² area in the SSA22 field using CFHT’s WIRCam (Puget et al. 2004) with a typical seeing of 0.6 arcsec. The SSA22 field is the widest contiguous field for which a wealth of multiwavelength data is available, most importantly *ugriz* from CFHTLS-Wide and *JK* from UKIDSS-DXS, see Fig. 2.

We use the LowOH2 filter ($\lambda_c = 1.187 \mu\text{m}$, $\Delta\lambda = 0.01 \mu\text{m}$) which can detect Ly α emission ($\lambda_0 = 121.6 \text{ nm}$) at $z = 8.76 \pm$

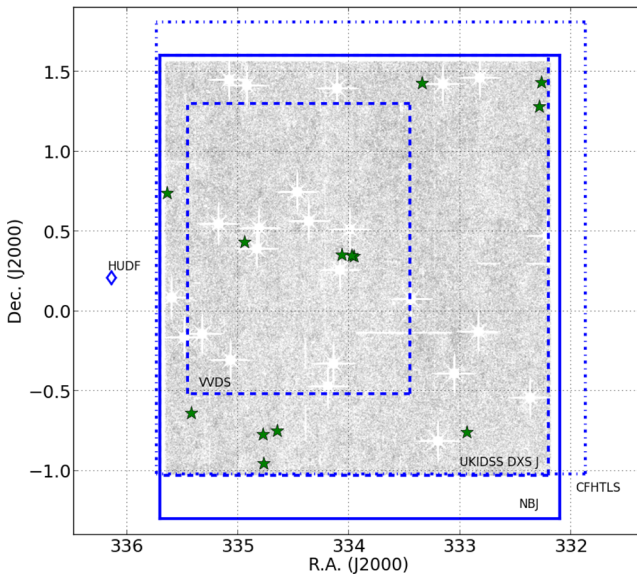


Figure 2. The surveyed area in the SSA22 field and overlap with other surveys. In grey, we show all detected NB $_J$ sources, where white stars indicate the positions of the brightest stars ($J < 10.5$). NB $_J$ represents the area of the survey presented here. For LAEs at $z = 8.76$, the surveyed area roughly corresponds to $\sim 40 \times 60 \text{ Mpc}$, with a depth of $\sim 180 \text{ Mpc}$ comoving. Our Ly α candidates are shown as green stars. The overlapping regions with CFHTLS W4 (*ugriz*), UKIDSS DXS (*JK*) (Lawrence et al. 2007) and VVDS ((spectro- z ; Le Fèvre et al. 2005) are shown. For comparison, we also plot the size of the *Hubble Ultra Deep Field*, which is ~ 3000 times smaller than the area of this survey.

0.04 in a comoving volume of $4.7 \times 10^6 \text{ Mpc}^3$. This is larger by at least half an order of magnitude compared to the largest previous survey. Detailed information on the observations, data reduction and general selection of emitters can be found in Sobral et al. (in preparation), but see also Sobral et al. (2013b). In this paper, we explore potential Ly α candidates in the sample of emitters.

2.1 Source extraction and survey limits

We use SExtractor (Bertin & Arnouts 1996) and detect $\sim 350\,000$ sources across the 10 deg² NB coverage. The 5σ AB-magnitude limit for the survey is $\text{NB}_J = 22.2$, corresponding to an effective emission-line flux limit of $7 \times 10^{-17} \text{ erg s}^{-1} \text{ cm}^{-2}$. This limit is computed by measuring the average background rms of the NB images in empty 2 arcsec diameter apertures, which is the aperture we use throughout the paper for all measurements. We note that because we use random aperture measurements, the rms that we measure already accounts for correlations in the noise. The limiting magnitude is converted to line-flux using the following formula:

$$F_{\text{line}} = \Delta\lambda_{\text{NB}_J} \frac{f_{\text{NB}_J} - f_J}{1 - (\Delta\lambda_{\text{NB}_J} / \Delta\lambda_J)}. \quad (1)$$

Here, F_{line} is the line-flux (also called Ly α flux), $\Delta\lambda_{\text{NB}_J}$ and $\Delta\lambda_J$ ($\Delta\lambda_J = 0.158 \mu\text{m}$) are the widths of the NB and broad-band filter, respectively, while f_{NB_J} and f_J are the respective flux densities. For the flux limit, we use the broad-band limiting magnitude. This effective flux limit corresponds to 75 per cent completeness.

3 NB SELECTION OF CANDIDATES

In order to identify Ly α candidates, we look for line-emitters which show the characteristics of a $z > 7$ source. These should have a Lyman break, which should occur between the z and J band, and a flat or blue $J - K$ colour to exclude very dusty, lower redshift galaxies with strong breaks (e.g. the 4000 Å break). In practice, we use the following criteria:

- (i) be selected as a line-emitter in Sobral et al. (in preparation; as described in Section 3.1 below);
- (ii) no detection in filters on the blue side of the J band (see Section 3.2.1);
- (iii) no visible detection in the stack of all optical bands (see Section 3.2.2);
- (iv) reliable excess between NB $_J$ and J (see Section 3.2.3);
- (v) $J - K \leq 0$ and a photometric redshift consistent with $z > 4$ (see Section 3.2.4).

3.1 Emission-line candidates

Emitters were selected using two criteria which quantify the excess the NB has over the broad-band. First, the observed equivalent width (EW) should be larger than 30 \AA , corresponding to a rest-frame Ly α EW of 3 \AA . Secondly, the Σ parameter (equation 2), which quantifies the significance of the NB excess compared to the noise (Bunker et al. 1995), should be larger than 3 (similar to Sobral et al. 2013a):

$$\Sigma = \frac{1 - 10^{-0.4(J - \text{NB}_J)}}{10^{-0.4(ZP - \text{NB}_J)} \sqrt{\pi r_{\text{ap}}^2 (\sigma_{\text{NB}_J}^2 + \sigma_J^2)}}, \quad (2)$$

where ZP is the zero-point of the photometry (25), r_{ap} is the radius of the apertures in pixels and σ the rms per pixel in each band. In case of non-detections in J , the detection limit was assigned. More detailed

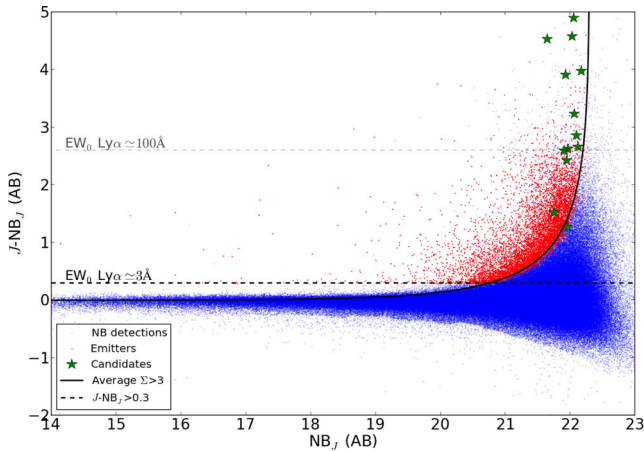


Figure 3. Colour–magnitude diagram for the NB_J sources. The $J-NB_J$ colour is corrected using the z band to compensate for the fact that the NB_J filter is not in the centre of the broad-band, see Sobral et al. (in preparation) for more details. The dotted horizontal line is for an observed EW of 30 \AA , which corresponds to $J-NB_J > 0.3$. The $\Sigma = 3$ curve is shown for the average depth of the survey. Emitters are shown in red, as they have EWs $> 30 \text{ \AA}$ and have a $\Sigma > 3$. The final $\text{Ly}\alpha$ candidates are shown with a green star and show a typical rest-frame EW (EW_0) of $\sim 100 \text{ \AA}$. The full sample of emitters is presented in Sobral et al. (in preparation).

information of the procedure and the full sample of emitters will be presented in Sobral et al. (in preparation). Using these criteria, out of the $\sim 350\,000$ NB_J sources individually detected, 6315 emitters were selected (see Fig. 3). This is after removing 2285 spurious sources and artefacts from bright stars by visual checks.

3.2 Selecting $\text{Ly}\alpha$ candidates at $z = 8.8$

3.2.1 Excluding lower redshift interlopers: optical broad-band photometry

A $z \sim 9$ source should be undetected in filters on the blue side of the J band, because the light at these wavelengths is absorbed by the IGM. This means that candidates must be undetected in the u , g , r , i and z bands. Data in these broad-bands is available from the Canada–France–Hawaii Telescope (CFHT) Legacy Survey (CFHTLS).¹ Deep data in the J and K bands are available from UKIDSS-DXS-DR10² ($J_{AB} \sim 23.4$, limit measured by the artificial star test). Two catalogues with sources in the optical bands of the CFHTLS were used. The first catalogue was the public CFHTLS-T0007 catalogue, in which sources were detected in the gri stack. The second catalogue (Kim et al., in preparation) contains 859 774 sources with photometric redshifts. It used J -band images from UKIDSS-DXS-DR10 for the detection of images. This catalogue is called the SSA22 catalogue and has depths of $(u, g, r, i, z, J, K) = (25.2, 25.5, 25.0, 24.8, 23.9, 23.4, 22.9)$. For the optical, these depths are taken from the public CFHTLS catalogue and correspond to 80 per cent completeness, for JK these are 90 per cent complete (Kim et al., in preparation).

The line-emitters were matched to the CFHTLS and SSA22 catalogues with a maximum 1 arcsec separation on the sky using TOPCAT (Taylor 2005). A list with candidates that followed the first criterion was made by clearing sources with magnitudes brighter than the limits in one or more of the optical bands. After this first criterion, 302 candidates remained.

¹ <http://www.cfht.hawaii.edu/Science/CFHTLS/>

² <http://www.ukidss.org/>

3.2.2 Visual check: optical stack

For line-emitters that passed the first criterion, thumbnails were made of the stack of the optical bands $ugriz$. This is necessary to reject sources which have flux in the optical which is too faint to be detected in a single band, but that will be revealed in the stack as it has an estimated depth of ~ 27 AB. Using the stack, sources with a detection in the optical (on the blue side of J) were identified and ruled out as $z = 8.8$ LAE. After this step, 40 candidates remained. Most of the candidates which were lost in this step are lower redshift contaminants such as $[\text{O II}]$ at $z = 2.2$, see Sobral et al. (in preparation). This is confirmed by their very red $J - K$ colours.

3.2.3 Visual check: narrow-band, broad-band and excess

Thumbnails are also made from the UKIRT J and K images and of the NB image itself (see Figs A1 and A2 in the appendix and e.g. Fig. 5). Sources are then visually checked again in all bands. By comparing the broad-band and NB image, we were able to confirm if the source demonstrates a true NB excess, instead of an excess caused by a boosted background. We also check whether the NB flux density is consistent with that of the broad-band J , because the broad-band includes the NB wavelength coverage. After all these visual checks, 25 candidates remained, as 15 were marked as spurious or unreliable.

3.2.4 Photometric redshifts

Self-consistent photometry for the candidates was made by running SExtractor in dual-image mode on the thumbnails, using the NB image as the detection image. In the case of non-detections by SExtractor in any of the other bands, the limiting magnitudes of the catalogue (see Section 3.2.1) were assigned. Using this consistent set of fluxes of the candidates in different wavelengths, we were able to derive a photometric redshift using EAZY³ (Brammer, van Dokkum & Coppi 2008). Unfortunately EAZY doesn't have a template for strong $\text{Ly}\alpha$ emission; therefore, we create supplementary templates where we added this emission line to existing templates.

Some candidates at this point show a red $J - K$ colour and potentially very faint detections (below the 1σ limit) in the r , i or z band and are also not visible in the optical stack, indicating that these sources are likely very dusty lower redshift line-emitters. The emission line detected is in this case likely $[\text{O II}]$ at $z = 2.2$ and the break between z and J the 4000 \AA break, which can mimic the Lyman break. From the 25 candidates for which we obtained an SED, 12 were marked as lower redshift contaminants. This left 13 candidates, which could not be further rejected without follow-up observations, see Table 1. We divide these candidates in different groups given below.

3.2.5 Different types of candidates

The candidates can be ordered in three different groups: (i) candidates with detections in NB_J , J and K , (ii) candidates with NB_J and J detections and (iii) candidates with only strong NB_J detections. The measured magnitudes and computed quantities for individual candidates can be seen in Table A1 in the appendix, which also shows how the candidates are grouped. The first group contains the two

³ <http://www.astro.yale.edu/eazy/>

Table 1. Number of candidate LAEs at $z = 8.8$ after each step and fractions of lower redshift interlopers out of the 302 sources without optical detection.

Step	Number
Line-emitters	6315
No optical detection	302
No detection in optical stack	40
Believable excess, NB _J , J detections	25
Max number of Ly α candidates	13
With robust constraints	2
Fraction of H β /[O III]	0.36
Fraction of [O II]	0.23
Fraction of $z \sim 3-6$ emission lines	0.13
Fraction of $z < 0.8$ emission lines	0.18
Fraction of Ly α candidates	0.10

most robust sources with detections in J ($>5\sigma$), best constrained $iz - J$ break, robust blue $J - K$ colours and best constrained SED, see Figs 4 and 5. The second group consists of three candidates with both NB_J and J , while the third group consists of 10 possible candidates with weak SED constraints and fainter JK detections (see Fig. 4). Thumbnails for all candidates are shown in Figs A1 and A2.

3.2.6 Statistical likelihood

In order to further investigate our selection, we stacked the thumbnails in all bands for the two robust candidates with best-constrained broad-band photometry, the 11 other candidates and the dominant lower redshift interlopers with individual photometric redshift of ~ 2 . We measured the stacks with the NB image as detection image and ran EAZY to compute photometric redshifts. As can be seen in Fig. 4, red and dusty galaxy templates are favoured for our lower redshift interlopers. Fig. 4 also shows that the Ly α candidates are best fitted by the high-redshift solution, even though they show the

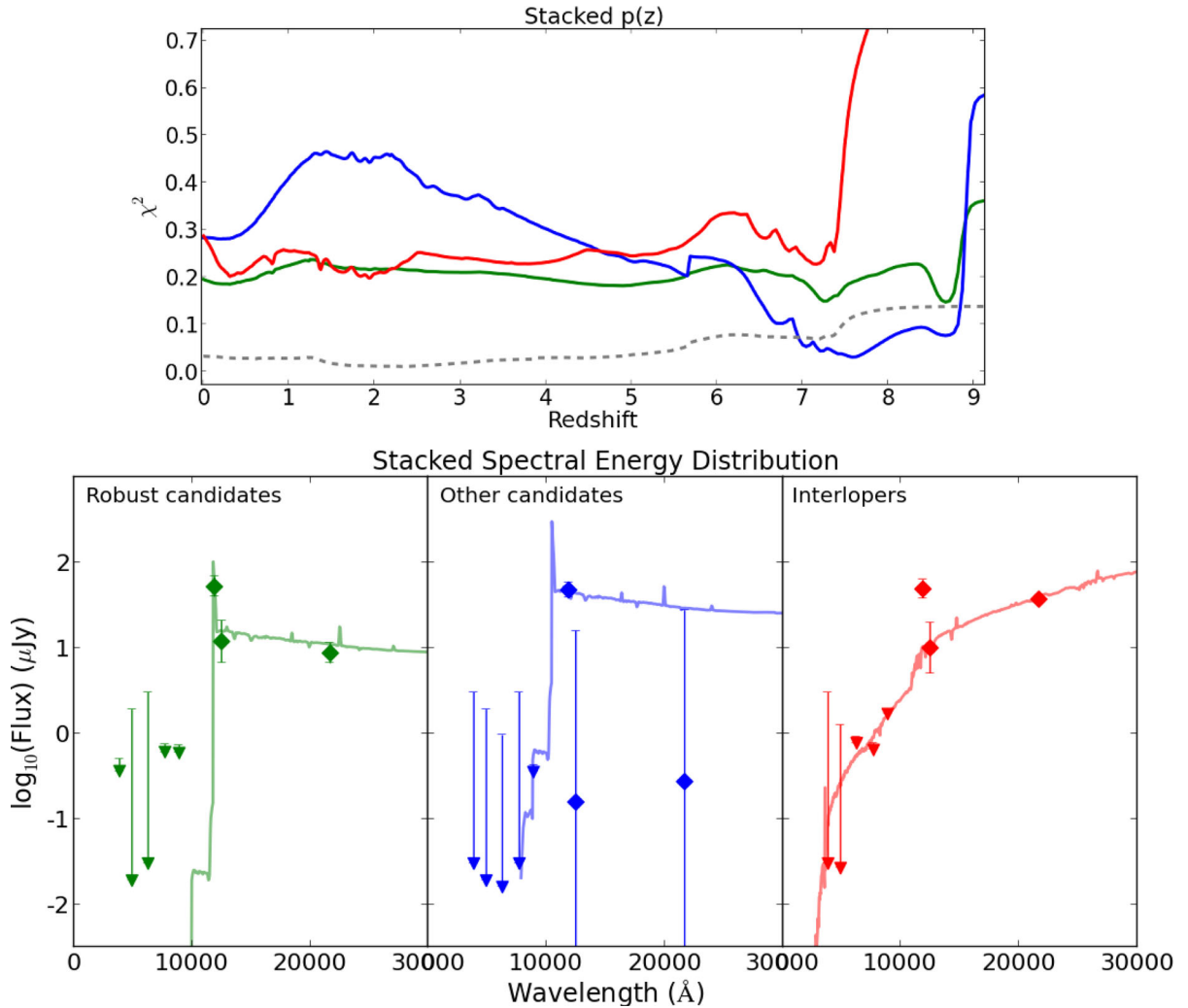


Figure 4. Top panel: stacked redshift- χ^2 distribution for the three samples. Bottom panel: stacked SED of our robust Ly α candidates ($z_{\text{phot}} = 8.7$; left, green), the other Ly α candidates ($z_{\text{phot}} = 7.2$; centre, blue) and the dominant lower redshift interlopers ($z_{\text{phot}} = 2.1$; right, red). For the interlopers, the fits clearly prefer a dusty, red galaxy solution. In the top panel, dashed grey shows the redshift- χ^2 distribution of the most robust candidates for running EAZY without adding the Ly α flux. The degeneracy between the [O II] and high-redshift solution can clearly be seen in all three subsets. For the Ly α candidates, the high-redshift solution is preferred.

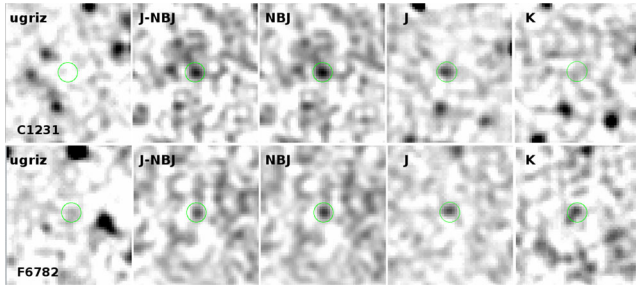


Figure 5. Thumbnail images for the most robust $\text{Ly}\alpha$ candidates. IDs C1231 and F6782. The size of the thumbnails is $15 \text{ arcsec} \times 15 \text{ arcsec}$. The image on the left shows the stack of all the optical bands (*ugriz*), clearly there are no detections. The second image shows the excess, which consists of the difference between *J* and NB_j . The right image shows the *K* band. This is mainly used to check whether the source is not a very dusty emitter at a lower redshift, for example $\text{H}\beta/[\text{O III}]$ at $z \sim 1.4$ or $[\text{O II}]$ at $z \sim 2.2$, as such a source would be expected to have $J - K > 0$.

same degeneracy as the lower redshift interlopers. By adding the strong $\text{Ly}\alpha$ emission in the *EAZY* templates, solutions around $z = 8.8$ are preferred. Without the addition of the $\text{Ly}\alpha$ flux to the template spectra, the lowest χ^2 solutions would lie around $z \sim 2$, which can still be seen in the redshift- χ^2 distribution (Fig. 4, top panel).

3.3 Completeness

The procedure of selecting emission-line galaxies leads to potentially missing galaxies which have weak emission lines. To get an idea of how this influences the selection, we follow the procedure in Sobral et al. (2012, 2013a). We compute the completeness by using a sample of sources which are (1) not selected as line-emitters, but (2) are selected as high-redshift galaxies ($z > 3$, using photometric redshifts and *BzK* colours (Daddi et al. 2004)). This selection resulted in a sample of $\sim 20\,000$ sources in our field and mimics our selection of $\text{Ly}\alpha$ candidates very well. The second step is to add line-flux to these sources and re-apply the selection criteria for sources being line-emitters ($\text{EW} > 30 \text{ \AA}$, $\Sigma > 3$). This is done for increasing line-flux, and the number of sources which are being selected as line-emitters for each additional line-flux is counted. The completeness is the ratio of sources selected as emitters to the numbers in the original sample. This resulted in a completeness of ~ 90 per cent for the average $\text{Ly}\alpha$ line-flux of the candidates of $\sim 1 \times 10^{-16} \text{ erg s}^{-1} \text{ cm}^{-2}$ and of ~ 75 per cent for our detection limit of $7 \times 10^{-17} \text{ erg s}^{-1} \text{ cm}^{-2}$.

3.4 Lower redshift contaminants

Because of the large number of candidates with NB excess consistent with $z > 7$ (302) when relying just on broad-band photometry, it is possible to quantify the fraction of sources selected as $z > 7$ candidates this way which are actually lower redshift interlopers. Interlopers were identified by using the optical stack and photometric redshifts (significantly improved by *K*-detections). From the 302 sources, 13 were marked as $\text{Ly}\alpha$ candidates, while 15 were marked as unreliable/spurious. This left 274 interlopers, meaning that 90 per cent of high-redshift candidates which are selected just by using optical bands are lower redshift contaminants. Using the photometric redshifts available (see Sobral et al., in preparation) we find that from this 90 per cent contamination, 36 per cent are $\text{H}\beta/[\text{O III}]$ at $z = 1.4$, 23 per cent $[\text{O II}]$ at $z = 2.2$ and 13 per cent higher redshift emitters such as carbon or magnesium lines from AGN at $z \sim 3-6$,

while the remaining 18 per cent are likely very faint lower redshift sources like $\text{Pa}\gamma$ at $z = 0.09$ or He II at $z = 0.44$.

3.5 Properties of candidates

Based on the NB imaging, we find that our candidates are very luminous, with a median $\text{Ly}\alpha$ luminosity of $L_{\text{Ly}\alpha} \simeq 1.0 \times 10^{44} \text{ erg s}^{-1}$. Compared to lower redshift ($z \sim 3-6$) LAEs, the AGN fraction at these luminosities would be expected to be 100 per cent, although limited by small number statistics (Ouchi et al. 2008). On the other hand, sources with the similar or higher luminosities have already been found at $z = 6-7$, such as the $z = 6.6$ giant LAE *Himiko* (Ouchi et al. 2009, 2013), a triple major merger, with a $\text{Ly}\alpha$ luminosity of $3.9 \times 10^{43} \text{ erg s}^{-1}$. Mortlock et al. (2011) found a quasar at $z = 7.085$ with a $\text{Ly}\alpha$ luminosity of $\sim 10^{45} \text{ erg s}^{-1}$, 10 times brighter than our candidates.

The majority of candidates show high EW_{obs} of $\sim 1000 \text{ \AA}$ (see Table A1 in the appendix), which is comparable to lower redshift samples (e.g. Ouchi et al. 2010) and a strong $iz - J$ break (median $\gtrsim 2$). Because of the clear *J* detection, the strongest candidates have the lowest EW, but highest $iz - J$. We measured the full width at half-maximum (FWHM) of point sources around the candidates and of the stack of the robust candidates. The FWHM of point sources is $0.7 \pm 0.1 \text{ arcsec}$, while the stack has an FWHM of $0.9 \pm 0.1 \text{ arcsec}$. Converting this angular scale to a physical scale at $z = 8.8$ gives a physical size of $\sim 4 \text{ kpc}$, which is roughly one-fourth of the giant $z = 6.6$ LAE (Ouchi et al. 2013, which has extended $\text{Ly}\alpha$ emission), but a factor of 4 larger than ‘typical’ $z \sim 7-8$ LBG candidates (Oesch et al. 2010), so consistent with other observations.

All these properties estimated from the NB imaging are physically realistic, but only spectroscopic follow-up can confirm the sources as real LAEs.

4 SPECTROSCOPIC FOLLOW-UP

4.1 Spectroscopic observations and reduction

SINFONI (Eisenhauer et al. 2003; Bonnet et al. 2004) IFU observations of five $\text{Ly}\alpha$ candidates (C1231, F6782, F2615, F3932, L71, i.e. the two most robust and the three ones with highest significance, highest EW and lowest local noise properties) were taken as part of programme 092.A-0786(A) between 2013 October 9 and 31 in $< 0.8 \text{ arcsec}$ seeing and photometric conditions. Observations were made with the $8 \text{ arcsec} \times 8 \text{ arcsec}$ field of view and the *J* grating which has a resolving power of $\lambda/\Delta\lambda = 4000$. Each observation was split into eight 300 s exposures, and nodded around the target galaxy by $\sim 2 \text{ arcsec}$ for sky subtraction purposes. Target C1231 was observed for a total of 4.8 ks whilst the remaining four targets were observed for a total of 2.4 ks. To reduce the data, we used the SINFONI pipeline which extracts the slices, wavelength calibrates, flat-fields and sky-subtracts the data. Additional sky subtraction was carried out using the techniques described in Davies (2007). Flux calibration for each observation was carried out using standard star observations which were taken immediately before or after the science frames. To search for line emission from the $\text{Ly}\alpha$ candidates, we extract a one-dimensional spectrum from the data cube, collapsed over a region with diameter of 1.2 arcsec centred at the position of the NB source, and show these in Fig. 6. These spectra have a noise of $0.7-1.1 \times 10^{-18} \text{ erg s}^{-1} \text{ cm}^{-2} \text{ \AA}^{-1}$ over the wavelength range $1.182-1.192 \text{ \mu m}$ (the approximate range of the NB filter) and so a 3σ detection limit for a line of width $\text{FWHM} = 250 \text{ km s}^{-1}$ (typical for $z \sim 7$ LAEs of Ouchi et al. 2010) of $1 \times 10^{-17} \text{ erg s}^{-1} \text{ cm}^{-2}$.

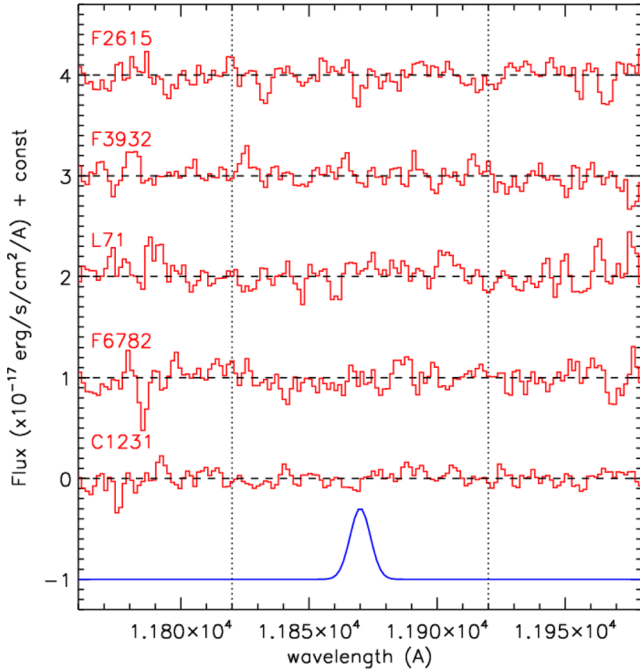


Figure 6. SINFONI IFU spectra from the five observed candidates (red). For illustrative reasons, a constant is added to all fluxes except C1231. The bottom row (blue) shows how our emission lines should have looked based on the NB estimated flux. The dashed vertical lines represent the width of the NB filter.

As Fig. 6 shows, none of the Ly α candidates are detected in emission by SINFONI, despite the flux limit of our NB survey which should have yielded $>7\sigma$ detections in all cases had emission lines been present. We also search for emission lines in the central 5 arcsec \times 5 arcsec coverage, but find nothing above 2σ . We must conclude that, although the two most robust candidates can still be real Lyman-break galaxies based on their broad-band magnitudes, they are excluded as luminous LAEs at $z = 8.8$. The others observed candidates are excluded as well. As these are the ones that resemble other candidates in the literature, their nature needs to be investigated (see Section 4.2). This has significant implications for other surveys.

One thing to note is that lower redshift line-emitters drawn from the same subsample (with similar excess-significance and estimated line-fluxes) were followed up with KMOS (Sobral et al. 2013b) and that strong emission lines were found in all of them.

4.2 Contaminations to high- z NB searches: spurious sources, variability & equatorial objects

This section gives an explanation for none of the candidates being confirmed. To do this, we again look at the different groups of candidates.

(i) We observed both candidates in the first group with the strongest NB $_J$, J and K photometry. The most likely explanation, given the relatively low Σ , but robust J and K (and given that the observations span different times), is that the excess is being boosted by noise. To estimate this, we look at the number of sources which are not selected as line-emitters, but fulfil the criteria of having no $ugriz$ and a blue $J - K$ colour and have reliable J - and K -detections, just as the two robust candidates in this group. From this number

(306), we can compute that when looking at 3Σ excess sources, we can expect 0.41 of these to have an excess by chance. The probability of getting both a 3.72Σ and a 3.03Σ source amongst the 306 is 1.1 per cent, this is low, but still possible.

(ii) We observed the most robust candidate with only NB $_J$ and J detections, and argue that, next to the possibility of the sources also being a statistical fluke, these sources are prone to variability. The time difference between the observations in J and NB $_J$ is of the order of 1–2 yr. Because candidates are selected as having a NB excess, variable sources which appear to be more luminous at the time when the NB observations are taken than at the time when the broad-band observations are taken, lead to a false NB excess. A rough estimate of variability is made by counting the number of sources with a very significant negative excess ($\Sigma < -7$ and $EW < -40\text{ \AA}$) and excluding stars. We investigate whether any of these negative excess sources (300 in total) is caused by variability. By careful visual inspection of these sources (to determine whether the negative excess is real), we conclude that a fraction of 81 per cent of these negative line-emitters is a variable source. The other negative excess sources are binary stars or extended objects selected as two different sources in one of the filters by SExtractor. So in total a fraction of 7×10^{-4} ($0.81 \times \frac{300}{350000}$) of the line-emitters is a variable source. This means that we can expect 4.4 line-emitters to be variable, possibly explaining the non-detection of our three Ly α candidates of this type.

(iii) The candidates which only rely on a NB detection have the chance of being a random noise spike, especially given that we observed a very wide area. We can get an estimate of the number of spurious sources in our survey by computing the total number of independent PSFs across the whole field. With a median seeing of 0.6 arcsec (Sobral et al. in preparation) and an effective area of 9 deg², we have 3.2×10^8 PSFs. We computed local noise estimates around the candidates by taking the standard deviation from the counts in 1000 000 2 arcsec-diameter apertures randomly distributed in ~ 1.7 arcmin² around the candidates, masking stars and other bright objects (NB $_J < 20$), see Table A1 in the Appendix. For the candidates in the third group, their median σ -detection is 5.44, based on the local noise. Using the number of PSFs, a total number of 8.5 spurious noise spikes is expected at this significance, which can explain the spectroscopic non-detection of the eight candidates in this group. We have done a visual analysis to remove clearly spurious sources, such as those near stars or in noisy regions, but this analysis might have missed these random noise peaks. Also, as the SSA22 field is equatorial, there is a slight chance that we observe small Solar system objects in our NB and this could also contaminate searches in other equatorial fields.

5 THE Ly α LF

5.1 Volume corrections

By assuming a top-hat filter profile, the comoving volume is 4.7×10^6 Mpc³, as our survey covered 9.0 deg², which is the area where the 10 deg² NB $_J$ survey overlaps with both the UKIDSS J and CFHTLS $ugriz$ surveys. The comoving volume must be corrected by including the dependence of the comoving volume on the luminosity, caused by the filter not being a perfect top-hat (e.g Sobral et al. 2009, 2013a). Making use of the derived luminosity limit of the NB survey (namely 7.3×10^{43} erg s⁻¹), it is possible to find the minimum luminosity for a source at a given redshift to be observed in the survey. For example, a source with a luminosity of 3.4×10^{44} erg s⁻¹ would be detected at redshifts between 8.723

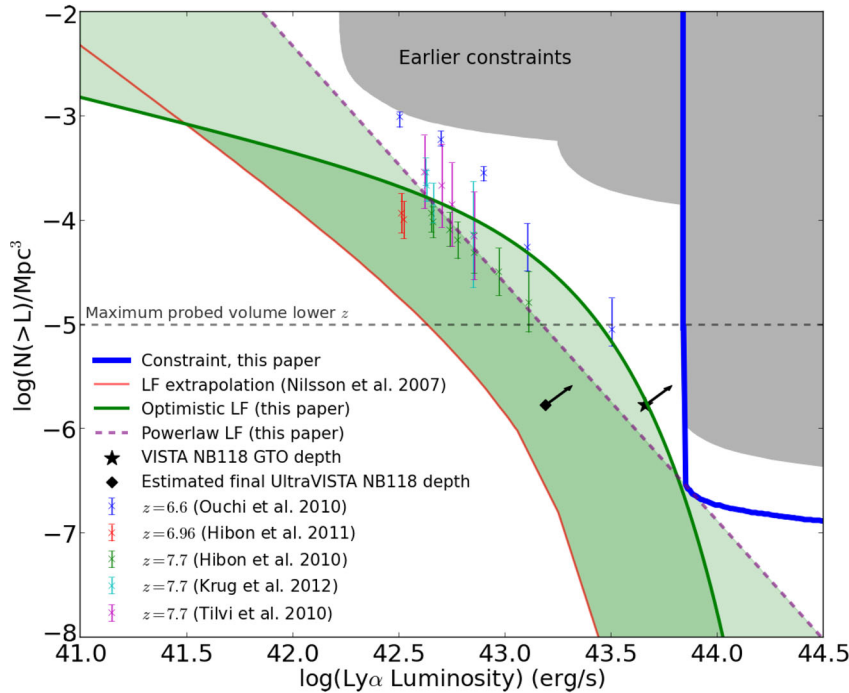


Figure 7. Constraint on the $\text{Ly}\alpha$ at $z \sim 9$ LF of this paper compared to LFs at lower redshifts, a scaled LF extrapolation and optimistic fitted upper limit LF. The thick blue line shows the new constraint, drawn from the non-detections in our survey (after spectroscopic follow-up). The new constraint improves previous ones by a factor of 5. The thick green line is an optimistic fitted Schechter function based on our observations and earlier observations at $z = 7.7$, while the magenta line shows a fitted power law. The red line is an extrapolation from LFs at lower redshift. The green area marks the region where we expect to observe LAEs, where there is a higher chance in the darker region. Also shown are the points from lower redshift NB searches. We plot the point of the depth of the finished VISTA NB118 GTO survey (Milvang-Jensen et al. 2013) and make a realistic estimate of what the depth will be of the ongoing UltraVista NB118 survey (McCracken et al. 2012).

Table 2. NB $\text{Ly}\alpha$ surveys at $z > 7$.

Reference	Area (arcmin ²)	Depth (10^{42} erg s ⁻¹)	z	No. LAE	Field
Ota et al. (2010)	4680	9.2	7	3	SXDS
Tilvi et al. (2010)	784	4	7.7	4	LALA Cetus
Hibon et al. (2010)	400	6	7.7	7	CFHT-LS D1
Hibon et al. (2011)	465	~1	6.96	6	COSMOS
Clément et al. (2012)	169	~2	7.7	0	Bullet, GOODS-S, CFHT-LS D4
Krug et al. (2012)	760	5.5	7.7	4	COSMOS
Willis & Courbin (2005)	6.25	20	~9	0	HDF South
Willis et al. (2008)	12	10	~9	0	Abell 1689, 1835, 114
Cuby et al. (2007)	31	13	8.8	0	GOODS
Sobral et al. (2009b)	5040	63	8.96	0	COSMOS, UDS
This paper	32 400	63	8.76	0	SSA22

and 8.816 due to the filter transmission and giving a corresponding comoving survey volume of $6.06 \times 10^6 \text{ Mpc}^3$.

5.2 Computing the LF

Following the non-detections in our spectroscopic follow-up, we put a constraint on the bright end of the $z = 8.8$ $\text{Ly}\alpha$ LF by probing to a $\text{Ly}\alpha$ luminosity of $10^{43.8} \text{ erg s}^{-1}$ over $4.7 \times 10^6 \text{ Mpc}^3$ (see Fig. 7). Using literature data from $z = 7.7$ LAE searches (see Table 2), we compute an optimistic upper limit to the LF, using all sources from earlier $z = 7.7$ surveys and our constraint as an upper limit. Although $z = 7.7$ – 8.8 seems a significant difference in redshift, the

difference in cosmic time is comparable to a sample of e.g. $z = 0.78$ – 0.82 . Fitting a Schechter function with a fixed faint-end slope α of -1.5 (following Ouchi et al. 2010), we find $\log_{10}(\Phi^*) = -4.21^{+0.11}_{-0.11}$ and $\log_{10}(L^*) = 43.10^{+0.03}_{-0.03}$. We also fit a simple power law with $\log_{10}(\Phi) = 93.3 - 2.28 \log_{10}(L)$. We note that these LFs should be interpreted as a very optimistic scenario, as none of the $z = 7.7$ sources have been confirmed spectroscopically.

5.3 Comparison with other surveys

Earlier searches for $\text{Ly}\alpha$ at $z \sim 9$ have put constraints on the LF. Cuby et al. (2007) and Willis et al. (2008) obtained too faint

magnitudes, but observed significantly smaller areas (~ 10 arcmin²). Sobral et al. (2009) is of the same depth as our current survey, but probed a factor of 5 smaller area. More searches have been conducted at a redshift of ~ 7.7 , which has not led to any spectroscopic confirmation, despite the recent attempts. For a summary, see Table 2.

Recently Jiang et al. (2013) followed up one $z = 7.7$ candidate, but they failed to confirm the line. Compared to our survey, this candidate was a factor 10 fainter and detected in a probed volume 200 times smaller than this work. None of the other candidates from the $z = 7.7$ searches have been confirmed spectroscopically so far. Faisst et al. (2014) also followed-up two of the best Krug et al. (2012) $z = 7.7$ candidates, finding no line emission, in line with our results. The majority of these $z = 7.7$ candidates rely on NB detections only, as our group (iii) candidates (Section 3.2.5) and we caution about these candidates being real, based on the arguments in Section 4.3.

5.4 Predictions for future and on-going surveys

Between $z \sim 6$ and 7, Ouchi et al. (2010) find negative evolution in the Ly α LF, caused mostly by a fainter L^* . It would be a logical step to further investigate this to even earlier times. In order to examine the evolution of the bright end of the LF, samples of luminous Ly α candidates would have to be compared with lower redshift samples. This is however impossible because the majority of searches only probes small survey areas (see Table 2). It is by no means certain that extrapolation (e.g. Nilsson et al. 2007) from results over smaller areas (and fainter LAEs) hold for large luminosities as those surveys miss the most luminous sources. As illustrated in Fig. 7, there is practically nothing known at densities $\log \Phi < -5$ at $z \sim 6-8$, but also not for $z \sim 5-6$ (Ouchi et al. 2008). LFs at $z < 6$ on the bright end are dominated by cosmic variance. The only way to overcome these problems is to conduct very wide (~ 10 deg²) NB searches for LAE at redshifts $z = 2-8$, as for example Subaru's Hyper Suprime Cam will be able to do over the next few years (Takada et al. 2012).

Future surveys such as the NB118 ($\lambda_c = 1.19$ μm , $\Delta\lambda = 12.3$ nm) UltraVista component (McCracken et al. 2012) will probe deeper than this work and should have a good chance of finding LAEs at $z \sim 9$, although their survey area will be smaller. Because of a smaller survey area, the survey will be less likely to find the most luminous sources and will be more affected by cosmic variance, which plays an important role in whether high-redshift LAEs can be observed due to reionization topology (e.g. Taylor & Lidz 2014). The completed VISTA NB118 GTO survey has probed 0.9 deg² to a line-flux of $4.4-5 \times 10^{-17}$ erg s⁻¹ cm⁻² (depending on reduction; Milvang-Jensen et al. 2013), which is already fainter than our current constraint (see Fig. 7). The ongoing UltraVISTA NB118 survey will probe the same area in a different part of the sky and its depth can be extrapolated from the finished survey. As the VISTA NB118 GTO survey had 12 per cent (12.33 h pixel⁻¹) of the total exposure time of the ongoing UltraVISTA NB118 survey (112 h pixel⁻¹; McCracken et al. 2012; Milvang-Jensen et al. 2013), we estimate the final depth assuming that the depth increases with $\sim t_{\text{exp}}^{0.5}$. Therefore, the final depth of the UltraVISTA NB118 survey will increase by a factor of ~ 2.9 , leading to an Ly α flux limit of $\sim 1.5-1.7 \times 10^{-17}$ erg s⁻¹ cm⁻².

Using our optimistic upper limit to the LF and the Nilsson et al. (2007) extrapolation as lower limit, we can estimate the number of LAEs that the UltraVista survey will detect (also see the marked green area in Fig. 7). For the GTO depth, this number is 0.001–

1.19 and for the estimated final UltraVista depth this is 0.19–23.35. When fitting a power-law LF to the $z = 7.7-8.8$ points, the current depth is expected to find 0.47 LAE, while the final depth can get to 6.00 LAEs. Since the UltraVista camera has 16 detectors with 16 different NB118 filters, there are small variations on the sky brightness from detector to detector, so some regions are shallower and some deeper (Milvang-Jensen et al. 2013). We used the median depths for the estimates above, but the numbers could vary because of a higher contribution from the deepest regions. Nevertheless, it is possible that even with the finished UltraVISTA NB118 survey, no $z = 8.8$ LAE will be found. On the other hand, our results clearly show how important it will be to spectroscopically follow-up any candidate arising from any similar survey.

6 CONCLUSIONS

We have conducted a very wide NB survey over 10 deg² in the near-infrared and identified 6315 line-emitters using a 1.19 μm NB filter. In this work, we identified possible $z = 8.8$ Ly α candidates in the sample of line-emitters and followed-up the strongest ones spectroscopically. The main conclusions are as follows.

- (i) A significant fraction (~ 300) of the line-emitters are consistent with being at high redshift ($z > 3$), of which some might be Ly α at $z = 8.76$. This NB survey increased the probed volume by half an order of magnitude compared to previous surveys and is thus sensitive to the rarest and most luminous sources.
- (ii) By doing careful visual checks of the robustness of the detections and by excluding line-emitters which are detected in any of the optical bands and which show a red $J - K$ colour, we find 13 possible Ly α candidates. We order them in different groups based on their broad-band photometric constraints. The two most robust candidates have reliable detections in NB, strongest constraints from photometric redshifts, $iz - J$ break and robust J -detections.
- (iii) 90 per cent of the high-redshift candidate line-emitters, selected on having no/very faint flux in the optical, are lower redshift interlopers. By including the K band and computing photometric redshifts, we find that approximately 40 per cent are H β /[O III] at $z = 1.4$, 25 per cent [O II] at $z = 2.2$ and 15 per cent are candidate AGN emission lines (e.g. carbon or magnesium) at $z \sim 3-6$, while the remaining are likely very faint lower redshift sources like Pa γ at $z = 0.09$ or He II at $z = 0.44$.
- (iv) Spectroscopic follow-up of the two most robust Ly α at $z = 8.8$ candidates, two sources with the largest EWs and another with brightest J failed to confirm these sources as line-emitters. This is probably caused by a combination of spurious sources, variability and (although unlikely) Solar system objects. This result has very strong implications to current and future candidates for LAEs at $z = 7.7$ and $z > 8$.
- (v) After the follow-up, we put the strongest constraints on the bright end of the LF with half an order of magnitude improvement in the probed volume and it could still mean little to no evolution in the luminous end.
- (vi) Using an optimistic upper limit to the LF and a lower redshift extrapolation, we estimate the number of LAEs that will be detected by the completed VISTA NB118 GTO survey to be between 0.001 and 1.19 with the current depth and to be between 0.19 and 23.35 for the estimated final depth of the ongoing UltraVista NB118 survey.
- (vii) Because of the lack of comparably wide surveys, it is difficult to study the evolution of the bright end of the LF and extrapolations from other considerably smaller surveys at lower redshifts

are unusable. Although the number density of LAEs is expected to decline at higher redshifts, this is not necessary the case for the bright end of the LF, because of the topology of reionization. It is therefore of utmost importance to study the bright end of the Ly α LF at lower redshifts in order to understand the evolution in the LF completely.

(viii) As our strongest candidates looked realistic in the images and had realistic physical properties based on the photometry, but still are not confirmed, we highlight the necessity for all other surveys to do this spectroscopic follow-up, especially when candidates are based on just a single-band detection. This has significant consequences for many similar and for deeper surveys, clearly pointing out that despite sources passing all tests, only spectroscopic observations can confirm them.

ACKNOWLEDGEMENTS

We thank the anonymous referee for the comments and suggestions which improved both the quality and clarity of this work. DS acknowledges financial support from the Netherlands Organisation for Scientific Research (NWO) through a Veni fellowship. IRS acknowledges support from STFC (ST/I001573/1), a Leverhulme Fellowship, the ERC Advanced Investigator programme DUSTYGAL 321334 and a Royal Society/Wolfson Merit Award. PNB acknowledges support from the Leverhulme Trust. JWK acknowledges the support from the Creative Research Initiative Program, no. 2008-0060544, of the National Research Foundation of Korea (NRF) funded by the Korean government (MSIP). JPUF and BMJ acknowledge support from the ERC-StG grant EGG5-278202. The Dark Cosmology Centre is funded by the Danish National Research Foundation. This work is based in part on data obtained as part of the UKIRT Infrared Deep Sky Survey. Based on observations obtained with MegaPrime/MegaCam, a joint project of CFHT and CEA/IRFU, at the Canada–France–Hawaii Telescope (CFHT) which is operated by the National Research Council (NRC) of Canada, the Institut National des Science de l’Univers of the Centre National de la Recherche Scientifique (CNRS) of France and the University of Hawaii. This work is based in part on data products produced at Terapix available at the Canadian Astronomy Data Centre as part of the Canada-France-Hawaii Telescope Legacy Survey, a collaborative project of NRC and CNRS. This work was only possible due to OPTICON/FP7 and the access that it granted to the CFHT telescope. The authors also wish to acknowledge the CFHTLS and UKIDSS surveys for their excellent legacy and complementary value – without such high-quality data sets, this research would not have been possible.

REFERENCES

Barton E. J., Davé R., Smith J.-D. T., Papovich C., Hernquist L., Springel V., 2004, *ApJ*, 604, L1
 Bertin E., Arnouts S., 1996, *A&AS*, 117, 393
 Bonnet H. et al., 2004, *The Messenger*, 117, 17
 Bouwens R. J., Illingworth G. D., Franx M., Ford H., 2007, *ApJ*, 670, 928
 Bouwens R. J. et al., 2011, *ApJ*, 737, 90
 Bouwens R. J. et al., 2013, *ApJ*, 765, L16
 Brammer G. B., van Dokkum P. G., Coppi P., 2008, *ApJ*, 686, 1503
 Brammer G. B., van Dokkum P. G., Illingworth G. D., Bouwens R. J., Labbé I., Franx M., Momcheva I., Oesch P. A., 2013, *ApJ*, 765, L2
 Bunker A. J., Warren S. J., Hewett P. C., Clements D. L., 1995, *MNRAS*, 273, 513
 Bunker A. J., Caruana J., Wilkins S. M., Stanway E. R., Lorenzoni S., Lacy M., Jarvis M. J., Hickey S., 2013, *MNRAS*, 430, 3314

Caruana J., Bunker A. J., Wilkins S. M., Stanway E. R., Lorenzoni S., Jarvis M. J., Elbert H., 2013, preprint ([arXiv:1311.0057](https://arxiv.org/abs/1311.0057))
 Cen R., Haiman Z., 2000, *ApJ*, 542, L75
 Clément B. et al., 2012, *A&A*, 538, A66
 Cowie L. L., Hu E. M., 1998, *AJ*, 115, 1319
 Cuby J.-G., Hibon P., Lidman C., Le Fèvre O., Gilmozzi R., Moorwood A., van der Werf P., 2007, *A&A*, 461, 911
 Curtis-Lake E. et al., 2012, *MNRAS*, 422, 1425
 Daddi E., Cimatti A., Renzini A., Fontana A., Mignoli M., Pozzetti L., Tozzi P., Zamorani G., 2004, *ApJ*, 617, 746
 Davies R. I., 2007, *MNRAS*, 375, 1099
 Eisenhauer F. et al., 2003, in Iye M., Moorwood A. F. M., eds, *Proc. SPIE Conf. Ser. Vol. 4841, Instrument Design and Performance for Optical/Infrared Ground-based Telescopes*. SPIE, Bellingham, p. 1548
 Ellis R. S. et al., 2013, *ApJ*, 763, L7
 Faisst et al., 2014, preprint ([arXiv:1402.3604](https://arxiv.org/abs/1402.3604))
 Fan X. et al., 2006, *AJ*, 132, 117
 Finkelstein S. L., Rhoads J. E., Malhotra S., Grogin N., 2009, *ApJ*, 691, 465
 Finkelstein S. L. et al., 2012, *ApJ*, 756, 164
 Finkelstein S. L. et al., 2013, *Nature*, 502, 524
 Fontana A. et al., 2010, *ApJ*, 725, L205
 Fynbo J. U., Møller P., Thomsen B., 2001, *A&A*, 374, 443
 Fynbo J. P. U., Ledoux C., Møller P., Thomsen B., Burud I., 2003, *A&A*, 407, 147
 Guhathakurta P., Tyson J. A., Majewski S. R., 1990, *ApJ*, 357, L9
 Hibon P. et al., 2010, *A&A*, 515, A97
 Hibon P., Malhotra S., Rhoads J., Willott C., 2011, *ApJ*, 741, 101
 Hu E. M., McMahan R. G., 1996, *Nature*, 382, 231
 Hu E. M., Cowie L. L., McMahan R. G., 1998, *ApJ*, 502, L99
 Hu E. M., Cowie L. L., McMahan R. G., Capak P., Iwamuro F., Kneib J.-P., Maihara T., Motohara K., 2002, *ApJ*, 568, L75
 Hu E. M., Cowie L. L., Capak P., McMahan R. G., Hayashino T., Komiyama Y., 2004, *AJ*, 127, 563
 Iiev I. T., Shapiro P. R., McDonald P., Mellema G., Pen U.-L., 2008, *MNRAS*, 391, 63
 Iye M. et al., 2006, *Nature*, 443, 186
 Jiang L., Bian F., Fan X., Krug H. B., McGreer I. D., Stark D. P., Clément B., Egami E., 2013, *ApJ*, 771, L6
 Kashikawa N. et al., 2006, *ApJ*, 648, 7
 Komatsu E. et al., 2011, *ApJs*, 192, 18
 Krug H. B. et al., 2012, *ApJ*, 745, 122
 Lawrence A. et al., 2007, *MNRAS*, 379, 1599
 Le Fèvre O. et al., 2005, *A&A*, 439, 845
 Lehnert M. D. et al., 2010, *Nature*, 467, 940
 Lord S., 1992, NASA Technical Memorandum 103957: A New Software Tool for Computing Earth’s Atmospheric Transmission of Near- and Far-infrared Radiation. NASA, Washington, DC
 McCracken H. J. et al., 2012, *A&A*, 544, A156
 McLure R. J. et al., 2011, *MNRAS*, 418, 2074
 McLure R. J. et al., 2012, *VizieR Online Data Catalog*, 741, 82074
 Malhotra S., Rhoads J. E., 2002, *ApJ*, 565, L71
 Malhotra S., Rhoads J. E., 2004, *ApJ*, 617, L5
 Milvang-Jensen B. et al., 2013, *A&A*, 560, A94
 Mortlock D. J. et al., 2011, *Nature*, 474, 616
 Nilsson K. K., Orsi A., Lacey C. G., Baugh C. M., Thommes E., 2007, *A&A*, 474, 385
 Oesch P. A. et al., 2010, *ApJ*, 709, L21
 Oesch P. A. et al., 2012, *ApJ*, 759, 135
 Oesch P. A. et al., 2013, *ApJ*, 773, 75
 Ono Y. et al., 2012, *ApJ*, 744, 83
 Ota K. et al., 2010, *ApJ*, 722, 803
 Ouchi M. et al., 2003, *ApJ*, 582, 60
 Ouchi M. et al., 2008, *ApJS*, 176, 301
 Ouchi M. et al., 2009, *ApJ*, 696, 1164
 Ouchi M. et al., 2010, *ApJ*, 723, 869
 Ouchi M. et al., 2013, *ApJ*, 778, 102
 Pentericci L. et al., 2011, *ApJ*, 743, 132
 Pritchett C. J., 1994, *PASP*, 106, 1052

Puget P. et al., 2004, in Moorwood A. F. M., Iye M., eds, Proc. SPIE. Conf. Ser. Vol. 5492, Ground-based Instrumentation for Astronomy. SPIE, Bellingham, p. 978

Rhoads J. E., Malhotra S., Dey A., Stern D., Spinrad H., Jannuzi B. T., 2000, ApJ, 545, L85

Rhoads J. E. et al., 2003, AJ, 125, 1006

Rhoads J. E. et al., 2004, ApJ, 611, 59

Schenker M. A., Stark D. P., Ellis R. S., Robertson B. E., Dunlop J. S., McLure R. J., Kneib J.-P., Richard J., 2012, ApJ, 744, 179

Shimasaku K. et al., 2006, PASJ, 58, 313

Sobral D. et al., 2009, MNRAS, 398, L68

Sobral D., Best P. N., Matsuda Y., Smail I., Geach J. E., Cirasuolo M., 2012, MNRAS, 420, 1926

Sobral D., Smail I., Best P. N., Geach J. E., Matsuda Y., Stott J. P., Cirasuolo M., Kurk J., 2013a, MNRAS, 428, 1128

Sobral D. et al., 2013b, ApJ, 779, 139

Steidel C. C., Giavalisco M., Dickinson M., Adelberger K. L., 1996, AJ, 112, 352

Takada M. et al., 2012, preprint (arXiv:1206.0737)

Taniguchi Y. et al., 2005, PASJ, 57, 165

Tanvir N. R. et al., 2009, Nature, 461, 1254

Taylor M. B., 2005, in Shopbell P., Britton M., Ebert R., eds, ASP Conf. Ser. Vol. 347, Astronomical Data Analysis Software and Systems XIV. Astron. Soc. Pac., San Francisco, p. 29

Taylor J., Lidz A., 2014, MNRAS, 437, 2542

Thommes E., Meisenheimer K., Fockenbrock R., Hippelein H., Roeser H.-J., Beckwith S., 1998, MNRAS, 293, L6

Thompson D., Djorgovski S., Beckwith S. V. W., 1994, AJ, 107, 1

Thompson D., Djorgovski S., Trauger J., 1995, AJ, 110, 963

Tilvi V. et al., 2010, ApJ, 721, 1853

Treu T., Schmidt K. B., Trenti M., Bradley L. D., Stiavelli M., 2013, ApJ, 775, L29

Vanzella E. et al., 2011, ApJ, 730, L35

Willis J. P., Courbin F., 2005, MNRAS, 357, 1348

Willis J. P., Courbin F., Kneib J.-P., Minniti D., 2008, MNRAS, 384, 1039

APPENDIX A: LYMAN α CANDIDATE DATA

Table A1. List of Lyman α candidates. Candidates observed with SINFONI are marked with an *. The first two are the candidates which are marked as being most robust. The next three also seem to have J -detections, while the last group relies mostly on their NB $_J$ detection. The magnitudes are in AB and estimated with the NB as detection image. All optical measurements are on the noise level, as are some J and K measurements. The limit is assigned for these non-detections. In the case of believable detections, we measured NB $_J$, J and K in single mode as this is less prone to astrometric errors. Δ NB $_J$, ΔJ and ΔK are the 1σ magnitude errors by SEXTRACTOR. EW $_{\text{obs}}$ is in \AA and a lower limit is assigned for non-detection in J . The excess-significance Σ is estimated from single-mode photometry of the NB $_J$ and J band, with a local lower limit for the non-detections. $\sigma_{\text{NB,local}}$ is the significance level in 2 arcsec diameter aperture measurements from the local (~ 1.7 arcmin²) area around the candidates. Luminosities are based on a redshift of $z = 8.76$. The photometric redshifts are calculated with EAZY. z_{phot} includes the NB filter and an artificial Lyman α template, 1σ errors are shown. It should be noted however that these are largely unconstrained, especially for the candidates in the third group.

ID	RA (J2000)	Dec. (J2000)	u	g	r	i	z	NB $_J$	Δ NB $_J$	J	ΔJ	K	ΔK	EW $_{\text{obs}}$ (\AA)	Σ	$\sigma_{\text{NB,local}}$	L $_{\text{Ly}\alpha}$ (10 ⁴⁴ erg s ⁻¹)	z_{phot}
C1231*	334.642	-0.751	>25.2	>25.5	>25.0	>24.8	>23.9	21.75	0.21	23.32	0.22	24.01	0.55	450	3.72	10.32	1.19	8.68 ^{+0.08} _{-0.07}
F6782*	333.335	1.426	>25.2	>25.5	>25.0	>24.8	>23.9	21.95	0.23	23.25	0.21	23.22	0.23	219	3.03	8.09	0.90	8.66 ^{+0.06} _{-1.87}
F2615*	334.768	-0.775	>25.2	>25.5	>25.0	>24.8	>23.9	21.94	0.28	24.38	0.59	>22.9	-	401	3.45	4.30	1.18	0.73 ^{+0.55} _{-0.22}
C1591	334.939	0.429	>25.2	>25.5	>25.0	>24.8	>23.9	21.97	0.26	24.63	0.69	>22.9	-	604	3.65	6.16	1.18	6.81 ^{+0.13} _{-0.56}
C83	332.282	1.28	>25.2	>25.5	>25.0	>24.8	>23.9	21.90	0.24	24.54	0.64	>22.9	-	2108	3.86	9.94	1.25	6.99 ^{+1.07} _{-0.13}
C803	333.949	0.341	>25.2	>25.5	>25.0	>24.8	>23.9	22.06	0.26	>23.4	-	>22.9	-	>241	3.61	4.92	1.12	6.92 ^{+1.45} _{-1.45}
F1035	332.265	1.431	>25.2	>25.5	>25.0	>24.8	>23.9	21.95	0.21	>23.4	-	>22.9	-	>286	3.21	7.99	1.30	2.07 ^{+1.23} _{-1.56}
F1024	335.415	-0.643	>25.2	>25.5	>25.0	>24.8	>23.9	22.27	0.31	>23.4	-	>22.9	-	>165	3.28	7.51	1.04	8.68 ^{+0.03} _{-2.41}
F4815	333.968	0.345	>25.2	>25.5	>25.0	>24.8	>23.9	22.09	0.31	>23.4	-	>22.9	-	>231	3.21	4.79	1.06	7.56 ^{+0.34} _{-0.29}
F3932*	335.633	0.737	>25.2	>25.5	>25.0	>24.8	>23.9	21.61	0.17	>23.4	-	>22.9	-	>403	3.83	9.69	1.72	8.68 ^{+0.06} _{-0.06}
F2751	334.766	-0.958	>25.2	>25.5	>25.0	>24.8	>23.9	22.12	0.29	>23.4	-	>22.9	-	>224	3.11	5.96	1.03	1.62 ^{+0.64} _{-1.02}
F4818	334.056	0.350	>25.2	>25.5	>25.0	>24.8	>23.9	22.03	0.29	>23.4	-	>22.9	-	>253	3.64	4.86	1.21	7.28 ^{+0.58} _{-0.89}
L71*	332.934	-0.761	>25.2	>25.5	>25.0	>24.8	>23.9	22.06	0.30	>23.4	-	>22.9	-	>243	3.42	4.88	1.18	1.94 ^{+1.91} _{-1.41}

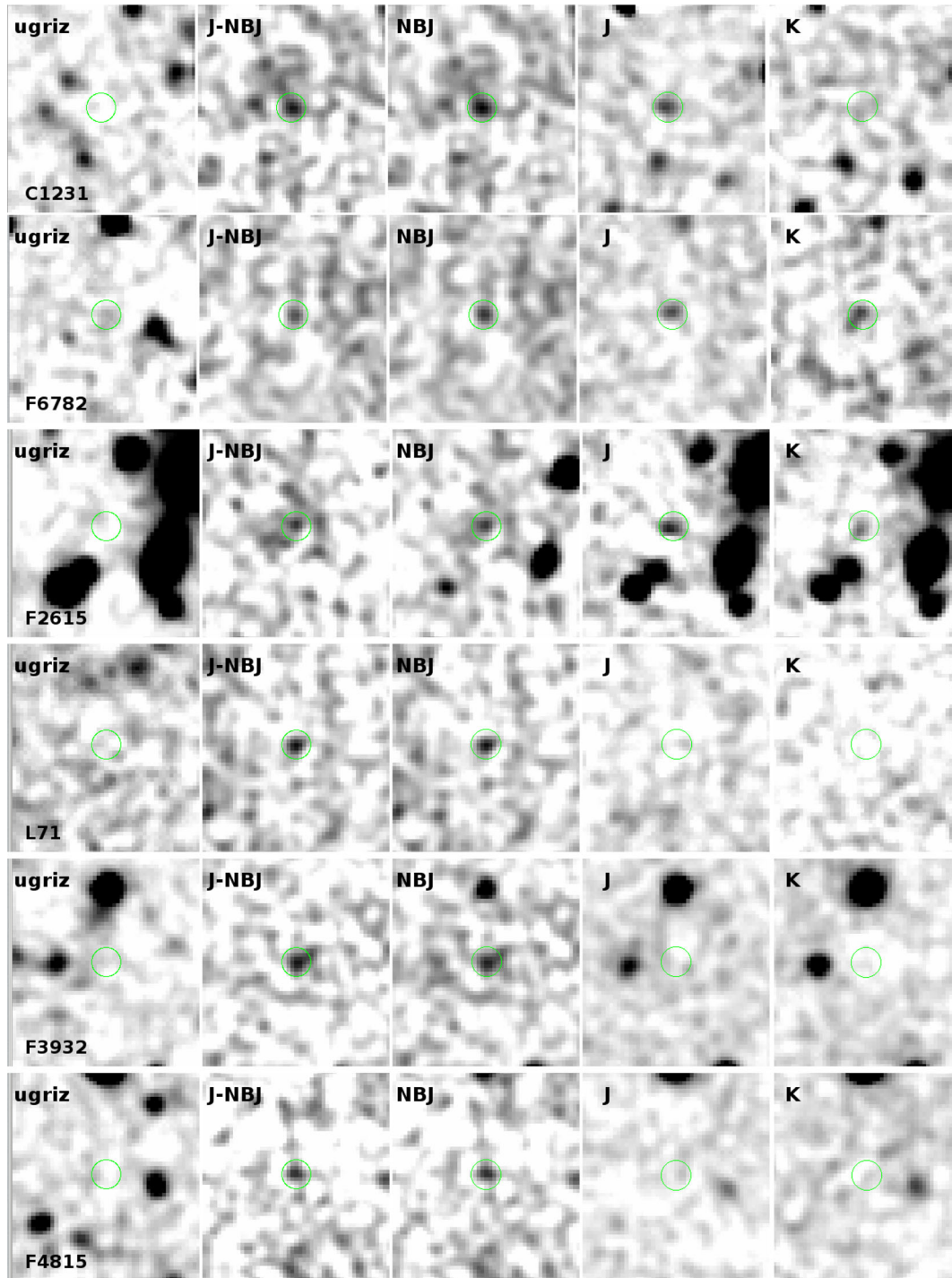


Figure A1. Top: thumbnails for the five Ly α candidates which were followed up spectroscopically. Bottom: one of the other candidates. Circles are placed at the centre position of the thumb, corresponding to the position of the detection in the NB. The angular scale of the thumbnails is 15 arcsec \times 15 arcsec.

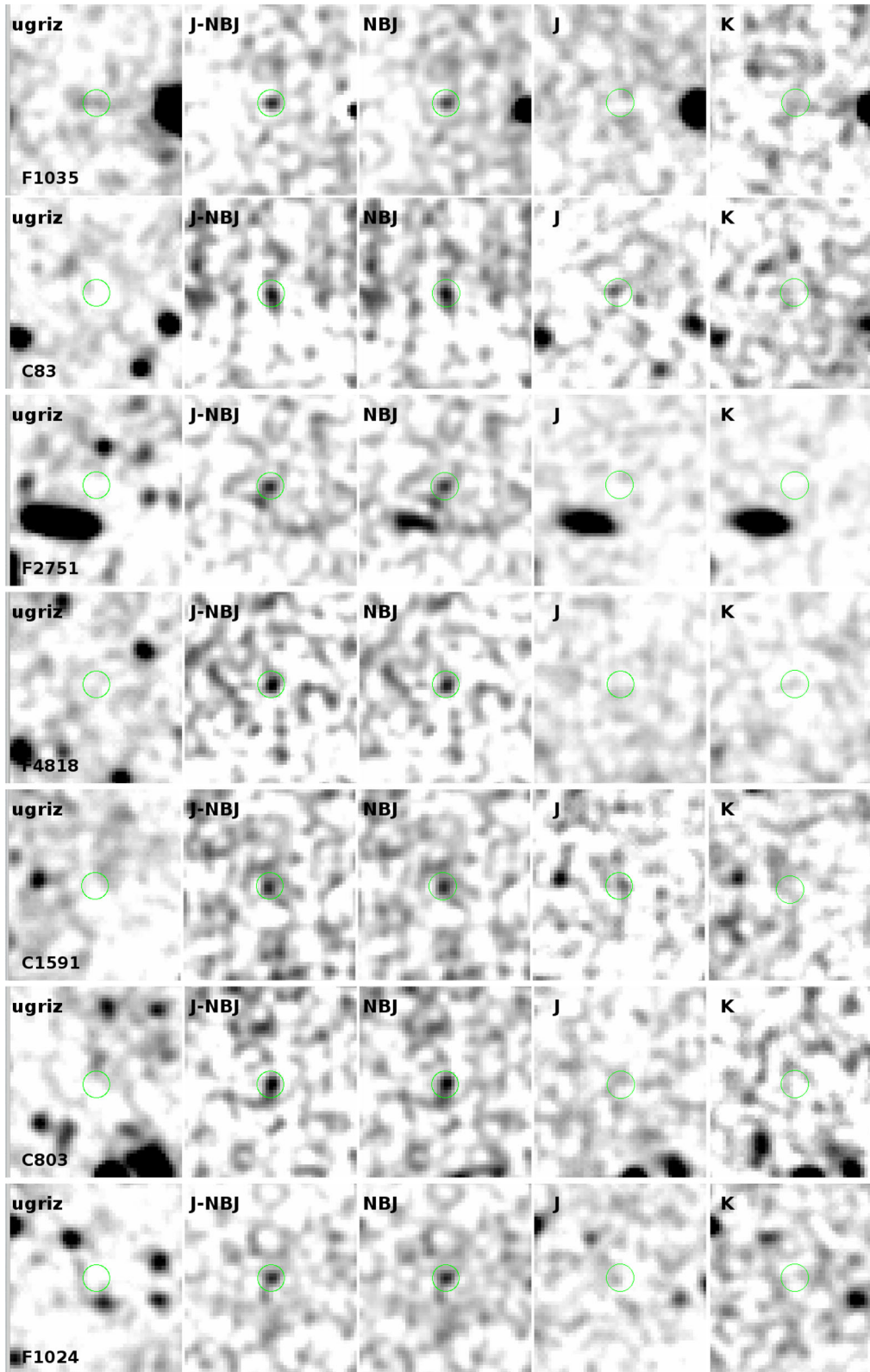


Figure A2. Thumbnails for the other seven Ly α candidates. Circles are placed at the centre position of the thumb, corresponding to the position of the detection in the NBJ. The angular scale of the thumbnails is 15 arcsec \times 15 arcsec.

This paper has been typeset from a $\text{\TeX}/\text{\LaTeX}$ file prepared by the author.